Cellular Bioeffect Investigations on Low-Intensity Pulsed Ultrasound and Sonoporation: Platform Design and Flow Cytometry Protocol

Xinxing Duan, Alfred C. H. Yu, *Senior Member, IEEE*, and Jennifer M. F. Wan

***Abstract*— At low-intensity levels, ultrasound can potentially generate therapeutic effects on living cells, and it can trigger sonoporation when microbubbles (MBs) are present to facilitate drug delivery. Yet, our foundational knowledge of low-intensity pulsed ultrasound (LIPUS) and sonoporation remains to be critically weak because the pertinent cellular bioeffects have not been rigorously studied. In this article, we present a population-based experimental protocol that can effectively foster investigations on the mechanistic bioeffects of LIPUS and sonoporation over a cell population. Walkthroughs of different methodological details are presented, including the fabrication of the ultrasound exposure platform and its calibration, as well as the design of a bioassay procedure that uses fluorescent tracers and flow cytometry to isolate sonicated cells with similar characteristics. An application example is also presented to illustrate how our protocol can be used to investigate the downstream cellular bioeffects of leukemia cells. We show that, with 1-MHz LIPUS exposure (with 29.1 J/cm^2 delivered acoustic energy density), variations in viability and morphology would be found among different types of sonicated leukemia cells (HL-60, Molt-4) in the absence and presence of MBs. Taken altogether, this article provides a reference on how cellular bioeffect experiments on LIPUS and sonoporation can be planned meticulously to acquire strong observations that are critical to establish the biological foundations for therapeutic applications.**

***Index Terms*— Cellular bioeffects, exposure platform design, flow cytometry, low-intensity pulsed ultrasound (LIPUS), microbubble (MB), sonoporation.**

I. Introduction

THE bioeffects of ultrasound pulsing at low-intensity level—an acoustic exposure range sometimes dubbed as low-intensity pulsed ultrasound (LIPUS)—have long been the subject of investigation [1], [2]. Perhaps the most widely known LIPUS-induced bioeffect that has been reported is the stimulation of bone regeneration, and it has long been leveraged to promote fracture healing [3], [4]. In contrast, when ultrasound is applied in the presence of microbubbles (MBs), acoustic cavitation would occur [5] to induce other types of bioeffects on living cells. In this latter scenario, cell membrane perforation is known to take place (a phenomenon that is commonly referred to as sonoporation) [6], and it has been widely considered as a physical way of enhancing drug delivery and gene transfer in biotherapeutics development [7]–[9]. Although the therapeutic potential of LIPUS and sonoporation is well recognized, the biological grounding in our current scientific understanding of these two phenomena has remained to be critically weak. In the case of LIPUS, its stimulatory benefits are sometimes controversial [10]–[12], and a stronger knowledge of the underlying biological mechanisms is necessary to corroborate the surmised therapeutic value [13], [14]. In the case of sonoporation, its practical efficiency is deemed to be mediocre [15], [16], and the pursuit of detailed knowledge on the pertinent cellular bioeffects is seemingly essential to devise strategies for improving the overall efficiency of this membrane perforation approach [17], [18].

From an experimental design standpoint, it is important to develop a meticulous methodology for cellular bioeffect investigations of LIPUS and sonoporation in order to avoid confounding factors in the interpretation of the derived results. Of particular importance is the proper design of an acoustic exposure platform whose *in situ* ultrasound field pressure and various intensity measures are well characterized as stipulated in bioeffect experiment reporting guidelines [19]. Based on this premise, acoustically coupled live cell imaging platforms have been constructed to gain insight into cellular morphology changes during ultrasound pulsing [20], [21] and acoustic cavitation [22]–[24]. Fluorescent and confocal imaging modes of these platforms have also been used to observe sonoporation-induced cytostructural remodeling [25], [26], intercellular interactions [27], calcium ion influx [28]–[30], transmembrane depolarization [31], and reactive oxygen species changes [32]. Alternatively, voltage clamp platforms have been developed to derive mean pore size estimates of individual sonoporation episodes through statistical fitting means [33]. For all of these platforms, they are well-suited to study single-cell dynamics during LIPUS exposure or over the course of a sonoporation episode. Nonetheless, they are inherently not intended for

Manuscript received October 24, 2018; accepted June 12, 2019. Date of publication June 17, 2019; date of current version August 26, 2019. This work was supported in part by the Natural Sciences and Engineering Council of Canada (CREATE-528202-2019), Canada Foundation for Innovation (36138), and the University of Hong Kong. *(Corresponding author: Alfred C. H. Yu.)*

X. Duan was with the School of Biological Sciences, The University of Hong Kong, Hong Kong. She is now with the Schlegel Research Institute for Aging, Waterloo, ON N2J 0E2, Canada, and also with the Department of Electrical and Computer Engineering, University of Waterloo, Waterloo, ON N2L 3G1, Canada (e-mail: xinxing.duan@uwaterloo.ca).

A. C. H. Yu is with the Schlegel Research Institute for Aging, Waterloo, ON N2J 0E2, Canada, and also with the Department of Electrical and Computer Engineering, University of Waterloo, Waterloo, ON N2L 3G1, Canada (e-mail: alfred.yu@uwaterloo.ca).

J. M. F. Wan is with the School of Biological Sciences, The University of Hong Kong, Hong Kong (e-mail: jmfwan@hku.hk).

Digital Object Identifier 10.1109/TUFFC.2019.2923443

population-based screening of ultrasound-induced bioeffects over a large group of cells.

Rational development of a population-based experimental protocol for ultrasound cellular bioeffect analysis, after all, requires careful considerations [34]. One major consideration to be taken into account is that all cell samples should be subjected to a relatively similar ultrasound exposure level. Yet, fulfilling this requirement is not trivial because many types of ultrasound exposure platforms are prone to undesired wave reflections [35] and standing waves [36], [37], while commercial sonication devices are known to generate significant acoustic field deviations that are not reported in the manufacturer datasheet [38]. Another caveat to remain vigilant about is that heterogeneity may exist in the cellular response to a given ultrasound exposure level, especially when MBs are present [39]. Without separating treated cells of different characteristics prior to running a prescribed bioassay, the resulting data and their analysis may inadvertently lead to spurious conclusions.

In this paper, we will stepwise present the design of an experimental protocol that seeks to investigate the mechanistic bioeffects of LIPUS and sonoporation over a cell population. This article is intended to echo a recent drive toward detailed reporting of methods and protocols in biomedical ultrasonics to foster repeatability of scientific findings [40]. In line with this endeavor, our specific contributions are threefold. First, we will describe various technical specifics on the ultrasound exposure platform and its calibration. Second, we will explain the key steps in a flow cytometry protocol that is designed to isolate sonicated cells with similar characteristics. Third, through presenting a case example on the topic of cell-type variations, we will illustrate how our protocol can be used in practice to conduct an original investigation on the downstream cellular bioeffects of different types of leukemia cells.

II. Ultrasound Instrumentation and Methods

Since an ultrasound-induced cellular bioeffect experiment should ideally yield correlative insight between ultrasound parameters and the bioassay outcomes, the ultrasound instrument should be designed with detailed consideration of the acoustic exposure level. In particular, such an instrument should meet three major requirements:

1) The *in situ* ultrasound exposure level should be known, and variations within the sample volume of interest should be well characterized [19].
2) Undesired wave reflections, including standing waves, should be avoided to reduce ultrasound field inhomogeneity in the exposure chamber [35], [36].
3) Ultrasound exposure parameters should be reported in detail in terms of pressure, intensity [19], and delivered energy [41].

For Requirement #3, reporting should not be done in units of voltage that is, after all, an electrical quantity, nor should it be done in units of wattage that is merely a global power quantity which does not give information about local fluctuations in the ultrasound field.

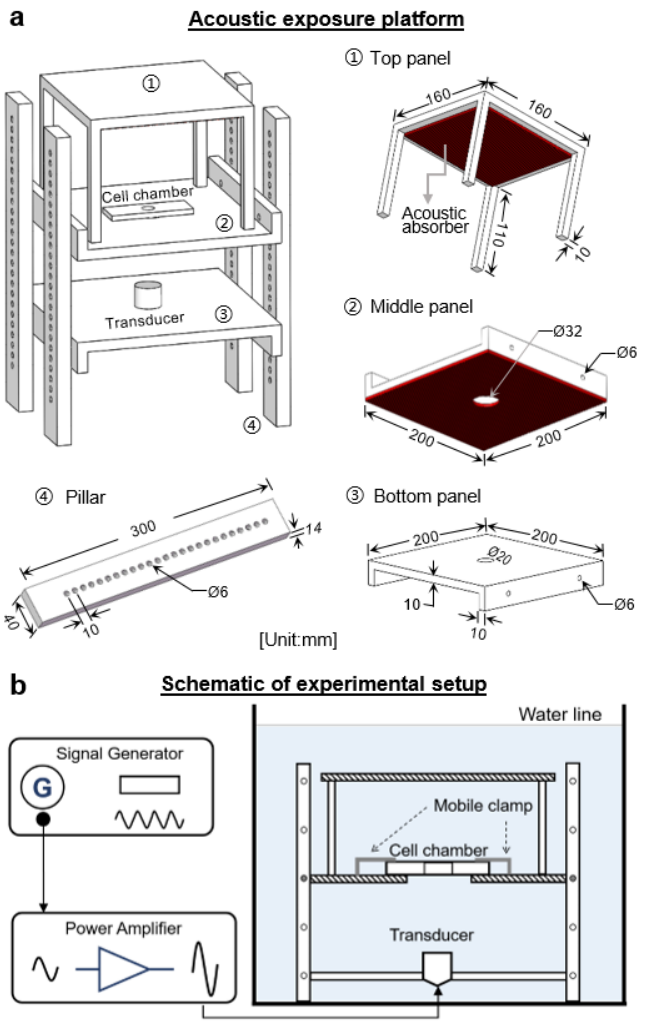

Fig. 1. Design of acoustic exposure platform. (a) Schematic of different structural components including their dimensions. (b) Illustration of the entire platform setup that includes transducer, signal generator, power amplifier, and the exposure platform immersed within a degassed water bath.

A. Acoustic Exposure Platform Design

Considering the key design requirements, we have devised an acoustic exposure platform as shown in Fig. 1. This setup involves the placement of a sealed cell chamber onto a platform that is immersed within a 37 °C degassed water tank, and ultrasound is delivered to the chamber in a direct line-of-sight configuration. Such an immersion-based platform has been characterized previously by simulations to yield a relatively homogeneous ultrasound field at the site of the ultrasound exposure chamber [35], thereby, satisfying Requirement #2. Its components were drafted using computer-aided design (CAD) software (SolidWorks; Dassault Systemes, Waltham, MA, USA), and they were fabricated at a machine shop using acrylic as the material. Note that a predecessor version of this platform with fewer design features and fewer field calibration details has been used previously by our group to pursue initial investigations of bioeffects induced by sonoporation [42], [43].

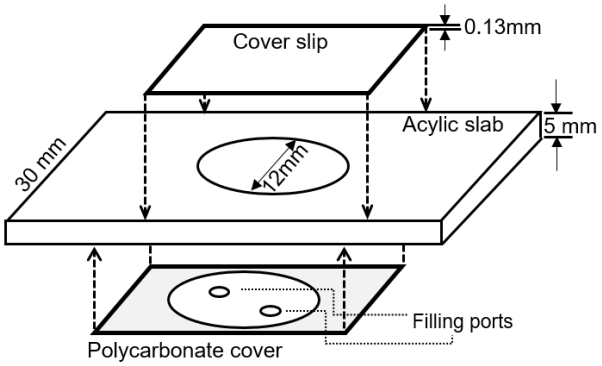

Fig. 2. Schematic of the customized cell chamber designed for containing cell samples during acoustic exposure.

In this setup, there are three acrylic platform panels. The bottom panel (length: 200 mm; width: 200 mm; height: 10 mm) serves as the holding panel for the ultrasound transducer, and at its center, there is a 20-mm diameter cylindrical bore that acts as a transducer holding slot. The middle panel (same dimension as the bottom panel) serves as the host platform for the sealed cell chamber. It has a 32-mm diameter bore at the center to facilitate ultrasound delivery to the cell chamber, and a pair of clamps is installed adjacent to this void to mount the chamber securely during ultrasound exposure. Its entire downfacing surface, except at the bore, is padded with a 5-mm-thick silicone rubber sheet (Norseal 9030; Saint-Gobain Performance Plastics, Herve, Belgium) to form an acoustic baffle against incident ultrasound waves. The height of the bottom and middle panels can be adjusted by fastening each panel to different positioning holes (with 1 cm spacing between holes) on the four vertical cuboid pillars, each of which is of 14 mm (length) $\times$ 40 mm (width) $\times$ 300 mm (height) in dimension. The distance between the bottom and middle panels was adjusted to 7 cm. This separation distance, corresponding to an axial location between the second-last and last maxima of the transducer's emission field, is empirically chosen as we have found that the corresponding lateral field profile spanned a small range of peak negative pressure values (shown in Section II-D). The top panel of this platform is a removable shield cover (length: 160 mm; width: 160 mm; height: 10 mm), and it is structurally supported by four leg poles (length: 10 mm; width: 10 mm; height: 110 mm). This top panel serves as an acoustic absorber as its downfacing surface is padded with a similar silicone rubber sheet to prevent incident ultrasound waves from reflecting toward the cell chamber. Note that the top panel is intentionally designed as a removable shield cover so that it can be conveniently withdrawn during operation and in turn allow the sealed cell chamber to be timely dismounted from the middle panel after ultrasound exposure.

B. Cell Chamber Design

The cell chamber is a sealable labware that we have custom designed. As shown in Fig. 2, it is in the form of a three-layer slab. The main layer in the middle is an 80 mm (length) $\times$ 30 mm (width) $\times$ 5 mm (height) acrylic cassette with a 12-mm diameter bore at its center. The top and bottom layers are respectively a 0.13-mm-thick glass coverslip (Bellco Glass, Inc., Vineland, NJ, USA) and a 0.18-mm-thick polycarbonate cover (HybriWell[1]; Invitrogen, Carlsbad, CA, USA) that effectively enclose the bore of the acrylic slide. Note that the thickness of these two layers is much thinner than the wavelength of 1-MHz ultrasound ($\sim$1.5 mm), so they would not act as significant interfacial boundaries that perturb ultrasound wave propagation when the cell chamber is mounted onto the exposure platform during operation. The enclosed bore of the cell chamber would give rise to a working volume of approximately 600 μL for holding the cell sample solution. There are two filling ports on the polycarbonate cover to facilitate the transfer of cell samples and culture medium. These ports would be securely sealed with adhesive tabs (A18211; Invitrogen) prior to mounting the cell chamber onto the acoustic exposure platform.

Prelab sterilization of the cell chamber is required to ensure that this labware can provide a sterile cell hosting environment during ultrasound exposure experiments. For this task, the fabricated cell chamber is stepwise rinsed in the following sequence prior to experimental use: three times with 75% ethanol, three times with deionized water (Milli-Q; MilliporeSigma, Burlington, MA, USA), and three times with phosphate buffered saline (PBS). Note that the cell chamber is a reusable labware and can be cleaned after the experiment to facilitate reuse. In our protocol, we adopted a postlab cleaning procedure that included these steps: 1) immersing the cell chamber in 10% (v/v) bleach for 1 h; 2) rinsing it with anionic detergent in warm water; 3) placing it in an ultrasonic cleaner (LS-02D; Limplus, Shenzhen, China) that was filled with deionized water for 3 min; and 4) washing it in triplicate with 75% ethanol and deionized water respectively. The cell chamber is also inspected under a microscope to ensure there were no observable contaminants or cracks. This labware is replaced if it is contaminated or broken.

C. Ultrasound Hardware

Our acoustic exposure platform can hold various types of immersible single-element transducers with different size and operating frequencies. For this paper, we have used a cylindrical ultrasound transducer with 1-MHz center frequency and 25-mm diameter (Advanced Devices, Wakefield, MA, USA). As shown in Fig. 1, the transducer was driven by the output of a 50-dB-gain broadband amplifier (2100L; E&I, Ltd., Rochester, NY, USA) that takes an arbitrary waveform input from a function generator (33120A; Agilent Technologies, Santa Clara, CA, USA). Note that the amplifier gain was fixed and not tunable. In line with our previous experiments [42], [43], the function generator was configured to deliver 100-cycle, 1-MHz pulses to the transducer after amplification. The generator's peak-to-peak output voltage was set to 600 mV; its pulse repetition frequency (PRF) was set to 1 kHz, thus, corresponding to a 10% duty cycle. The exposure period was defined as 30 s.

D. Ultrasound Field Characterization

To meet Requirement #1 mentioned in Section II-A, hydrophone measurements were conducted to characterize the

[1]Trademarked.

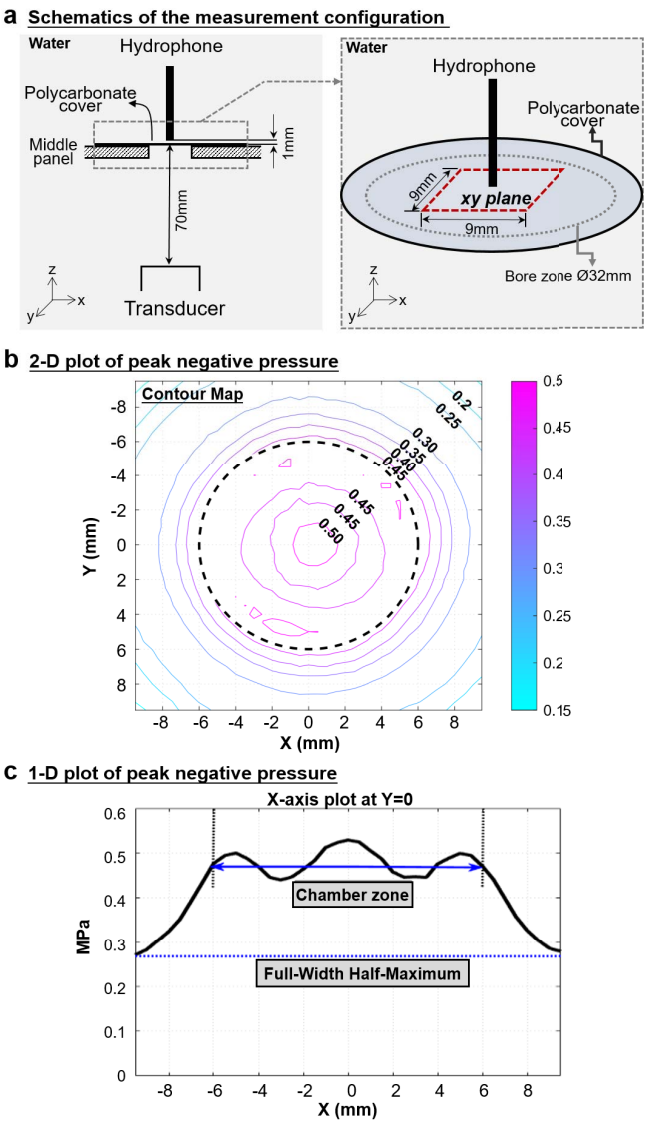

Fig. 3. Characterization of the *in situ* ultrasound field. (a) Schematic of the measurement configuration showing the placement of the hydrophone and polycarbonate cover. Peak negative pressure for the cross-sectional area (i.e., xy plane, $x = 18$ mm, $y = 18$ mm) was obtained from hydrophone measurements. (b) Contour map of the peak negative pressure for the cross-sectional area across the cell chamber (contour step = 0.05 MPa). (c) X-axis plot of the peak negative pressure along the $y = 0$ line. Note that the chamber zone was within the FWHM of the pressure field.

ultrasound field at the mounting site of the cell chamber within the acoustic exposure platform. These measurements were made using a needle hydrophone (HNR-0500; Onda Corporation, Sunnyvale, CA, USA) whose position was adjusted using an automated three-axis micropositioner (ASTS-01; Onda Corporation). To perform these measurements, the top panel of the acoustic exposure platform was first removed, and a polycarbonate cover was placed across the bore of the middle panel to include consideration of this cover's impact on the ultrasound field. Next, as shown in Fig. 3(a), the hydrophone tip was positioned close to the polycarbonate cover (1-mm separation to avoid contact). The ASTS-01 system's built-in software was then instructed to obtain a time plot of the measured acoustic pressure at the hydrophone tip's spatial position, and this process was automated to repeat across the cross-sectional plane to obtain a planar map of peak negative pressure.

Fig. 3(b) shows the corresponding contour map of the peak negative pressure on the hydrophone scan plane. The cell chamber boundary is denoted by the dashed circle in this plot. There was limited spatial variation in the peak negative pressure within the cell chamber. In particular, the pressure over this area was measured to be between 0.45 and 0.54 MPa, or a 1.6-dB fluctuation range which is less than the typical significance norm of 3 dB. As a further characterization, Fig. 3(c) shows a 1-D plot of peak negative pressure across the center line of the scanned surface. The fluctuation in acoustic pressure was a consequence of the fact that the chamber was axially located in the ultrasound transducer's near field, but the fluctuation range was found to be limited. The spatial-averaged peak negative pressure was found to be 0.50 MPa. The full-width-half-maximum (FWHM) of the spatial pressure distribution was found to be 19 mm, which is significantly larger than the cell chamber diameter.

E. Acoustic Exposure Calculations

To substantiate the notion of LIPUS, we have ensured that the ultrasound exposure delivered using our setup did not exceed most of the Food and Drug Administration's (FDA) upper limits for diagnostic ultrasound scanners [44] and related empirical findings from the literature [41]. Four acoustic exposure quantities have particularly been considered, as described below. These calculations also serve to meet Requirement #3 as mentioned in Section II-A.

1) Spatial-Peak, Pulse-Averaged (SPPA) Intensity: This quantity estimates the mean intensity of a single ultrasound pulse at the spatial peak of the planar pressure map. It can be calculated as follows based on well-known ultrasound physics formulas [45] for a given peak negative pressure at spatial peak $p_{\max}$ (0.54 MPa for our setup), medium density ρ and speed of sound c (993 kg/m^3 and 1512 m/s, respectively, for 37 °C water [35])

$$I_{\mathrm{SPPA}} = \frac{p_{\max}^2}{2\rho c}. \tag{1}$$

2) Spatial-Peak, Time-Averaged (SPTA) Intensity: This quantity derives the average intensity of the entire pulse repetition period at the spatial pressure peak. For a duty cycle δ (10% for our setup), it is defined as

$$I_{\mathrm{SPTA}} = \delta \frac{p_{\max}^2}{2\rho c} = \delta I_{\mathrm{SPPA}}. \tag{2}$$

3) Mechanical Index: This empirical quantity provides a general indication of the risk for cavitation activities to occur without the presence of synthesized gas nuclei. It is defined by the following formula [44] for a peak negative pressure expressed in MPa (0.54) and an ultrasound frequency f expressed in MHz (1 for our case)

$$\mathrm{MI} = \frac{p_{\max}}{\sqrt{f}}. \tag{3}$$

TABLE I
CALCULATED ACOUSTIC EXPOSURE VALUES AND THEIR COMPARISON AGAINST EMPIRICAL UPPER LIMITS

Acoustic Quantity	Limit	Calculated
Spatial-peak, pulse-averaged intensity, I_{SPPA} (W/cm^2)	190	9.71
Spatial-peak, time-averaged intensity, I_{SPTA} (W/cm^2)	0.72	0.97
Mechanical index, MI	1.9	0.54
Delivered acoustic energy density, E (J/cm^2)	42	29.1

4) Delivered Acoustic Energy Density: This quantity evaluates the ultrasound energy density deposited over the entire exposure period. For a total exposure period T (30 s in our case) [41], the delivered acoustic energy density can be found as follows:

$$E = \delta I_{\mathrm{SPPA}} T = I_{\mathrm{SPTA}} T. \tag{4}$$

Table I lists the FDA's upper limits for I_{SPTA}, I_{SPPA}, and mechanical index (MI) [44] and the empirical threshold for E as deduced from a past study [41]. The values calculated for our acoustic exposure setup are also shown in this table. All quantities except for I_{SPTA} are well within the upper limits. While I_{SPTA} was above the FDA limit by 35%, the resulting delivered acoustic energy density has previously been found to be a mild ultrasound dosage that would not lead to cellular damage in an MB-free medium [41]. As such, the exposure delivered by our setup can still be regarded to be within the LIPUS regime.

III. BIOEFFECT EXPERIMENT PROTOCOL

Our acoustic exposure platform may be used to investigate the bioeffects induced by LIPUS and sonoporation on various cell types. In this paper, a demonstration case is provided to illustrate our group's approach to analyze the bioeffects of a sonicated cell population using flow cytometry. Our example considers the bioeffects observed in both LIPUS-treated cells and sonoporated cells. It is a new experiment that aims to investigate cell-type variations in the observed bioeffects.

A. Cell Line Considerations

Since MBs tend to be injected intravenously in clinical practice, it would be reasonable for a sonoporation-induced bioeffect experiment to be designed to work with cells that are present in the vasculature, such as erythrocytes, leukocytes, and endothelial cells. Here, leukemia cells were chosen for our demonstration case as these cancerous cells tend to reside in the vasculature. Indeed, as sonoporation may have a repressive impact on living cells, the use of cancerous cells for a sonoporation bioeffect study would serve well as part of the experimental control since cancerous cells are known for their immortality and resistance against pro-apoptotic stress [46].

For our demonstration case, we have specifically chosen to work with two representative leukemia cell lines: HL-60 and Molt-4. Both cell lines were purchased from American Type Culture Collection (ATCC, Manassas, VA, USA). HL-60 cells (CCL-240; ATCC) are malignant cells derived from promyelocytic cells, while Molt-4 cells (CRL-1582; ATCC) are malignant cells differentiated from human T lymphoblasts. The two cell lines have been reported to exhibit diverse drug sensitivity and cell cycle progression features in responses to various stimulus or treatments [47], [48]. Accordingly, they may respond differently to the repressive stress of sonoporation.

B. Cell Culture Procedure

HL-60 and Molt-4 cells were routinely cultured in Roswell Park Memorial Institute (RPMI) 1640 medium (R8758; Sigma-Aldrich, St. Louis, MO, USA) in a culture dish and were supplemented with 10% fetal bovine serum (FBS, 30-2020; ATCC). The cell culture incubator was kept at 37 °C with 5% carbon dioxide (CO_2). Following ATCC's recommendations, their cell density was monitored to ensure that they did not exceed 10^6 cells/mL (for HL-60) or 2×10^6 cells/mL (for Molt-4) so that asynchronous and exponential cell growth can be maintained. Also, cells were subcultured once every 2 days (for Molt-4) or 3 days (for HL-60) as determined from the initial cell density and the doubling time of each cell line (24 h for HL-60; 30 h for Molt-4). Subculturing was conducted as follows. First, all cells were harvested in a sterilized 15-mL centrifuge tube (BDAA352196; BD Biosciences, East Rutherford, NJ, USA) and were centrifuged at 1000 rpm for 5 min. After that, supernatant RPMI medium was removed, and the cells were resuspended in fresh RPMI medium. Subsequently, the cell density was adjusted to ensure that the subculture concentration was within the vital range (10^5–10^6 cells/mL for HL-60; 2×10^5–2×10^6 cells/mL for Molt-4). Before using the cultured cells for ultrasound exposure studies, they were fed with fresh medium 1 day before the experiment.

C. Exposure Protocol Design

To analyze the bioeffects of LIPUS and sonoporation, the cell chamber was loaded with cultured cells, RPMI medium, tracer dyes, and MBs. This chamber, immediately after gentle agitation to ensure the loaded contents were uniformly distributed, was then mounted onto the acoustic setup for LIPUS exposure. A timeline of the key steps involved in this experimental protocol is shown in Fig. 4. In the first step, the 37 °C degassed water bath of the ultrasound exposure setup was prepared 1 h before LIPUS exposure. Then, after the cultured cells were resuspended at 2×10^7 cells/mL density, sonoporation tracer (calcein) and MBs (1:1 cell-to-bubble ratio) were added to the cell suspensions respectively at 10 and 3 min before ultrasound exposure. A set of experiments was also conducted without MBs to examine the standalone impact of LIPUS delivered by our acoustic platform. Subsequently, the loaded cell chamber was subjected to LIPUS exposure using our setup and parameters as described in Section II. After the exposure, cells were reincubated for 5 min, and then bioassays were conducted as described in Section III-D. Further remarks on the use of sonoporation tracer and MBs are presented below.

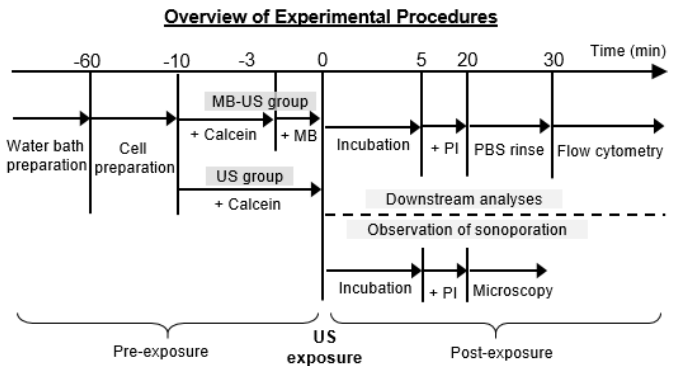

Fig. 4. Timeline of the experimental steps involved in the bioassay protocol. The timeline was set relative to the moment when ultrasound exposure was initiated. MB: microbubble; US: ultrasound; PI: propidium iodide; PBS: phosphate buffered saline.

1) Choice of Sonoporation Tracer: To help trace cells whose membrane has been disrupted via sonoporation, a fluorescent marker that is impermeable to a living cell should be added to the extracellular environment prior to exposure. If this fluorescent marker is found in the cytoplasm after ultrasound exposure, then it serves as evidence that the cell membrane has been disrupted during exposure, and in turn, it can be deduced that the cell has been sonoporated. For our demonstration case, calcein (C481; Invitrogen) was used as the sonoporation tracer. It is a 623-Da green-fluorescent macromolecule with a radius of 0.65 nm, an excitation band of 475–505 nm, and an emission band of 500–540 nm. During the experiment, calcein was added to the cell suspension at a concentration of 10 μM. Note that other types of fluorescent markers may be used as the sonoporation tracer. For instance, dextrans are polysaccharides with big molecular weights ($\geq$3 kDa), and they can be conjugated with fluorescein isothiocyanate to yield fluorescence. However, due to the relatively big size and weight, dextran might not always be effective in detecting small membrane disruptions [49]. Markers that are commonly used for cell viability detection may also be leveraged as a sonoporation tracer, because these dyes would only enter a cell to bind to nucleic acid contents if membrane integrity is disrupted. Examples include Sytox and propidium iodide (PI). These dyes were not used as a sonoporation tracer in our demonstration as cell viability was part of the flow cytometry analysis.

2) Considerations on MB Usage: If sonoporation is intended to be achieved through LIPUS exposure, it would be necessary to add synthetic MBs to the extracellular environment beforehand in order to make gas nuclei available for acoustic cavitation. For our experiment, commercial lipid-shelled MBs (TS-108; Targeson, San Diego, CA, USA; now acquired by TRUST Bio-Sonics, Hsinchu, Taiwan) were used as the artificial gas nuclei for sonoporation. These MBs were 2.09 μm in mean diameter, and less than 1.7% of them were larger than 5 μm according to the manufacturer's data. They were added at the same concentration as cell density, such that the cell-to-bubble ratio was 1:1 on average within the cell chamber. Most of the MBs ($>$99%) were found to have collapsed after 30-s LIPUS exposure period delivered by our setup, as deduced from empirical observations of the cell chamber under a bright-field microscope. This suggests that acoustic cavitation (most likely inertial cavitation) had taken place over the exposure period as necessary to facilitate sonoporation. Note that other types of MBs may be used, such as Definity (Lantheus Medical Imaging, Billerica, MA, USA) and Sonovue (Bracco Imaging, Manno, Switzerland). Similar variants like nanodroplets may also be used as sonoporation agents [50]. Another point to be noted is that the choice of cell-to-bubble ratio plays a significant role in the resulting sonoporation efficiency. As extensively analyzed in a previous study [41], a large ratio (i.e., a high number of cells per bubble) would result in limited instances of sonoporation, whereas a small ratio (i.e., many bubbles acting on one cell) would lead to irreversible cell damage by sonoporation. A 1:1 cell-to-bubble ratio is empirically deemed to provide a balance between triggering sonoporation and minimizing cell death. It should be emphasized that it is not necessary for bubbles to be attached to cells. Sonoporation may still be induced if the bubbles are within a critical distance from the cells, as shown earlier [51].

D. Post-Exposure Flow Cytometry

In order to properly analyze the bioeffects of LIPUS and sonoporation, it is important for bioessays to focus on cells that remain viable after exposure. Also, for studies involving sonoporation, the bioassays should be conducted only on cells that are confirmed to be viable and sonoporated. Accordingly, our experiment has included a post-exposure flow cytometry protocol to isolate sonicated cells in different categories based on their viability and whether they were sonoporated. For this task, a cell viability tracer (PI) was first added to the suspension 5 min after exposure. After another 15 min, the cells were used for post-exposure flow cytometry analysis. A fraction of samples was also imaged using live confocal microscopy to visualize calcein internalization. Details on each stage of the post-exposure experiment protocol are described as follows.

1) Use of Cell Viability Tracer: The addition of PI into the cell chamber 5 min after exposure effectively served to label cells whose membrane remained compromised at that time. These cells would be deemed as nonviable since post-sonoporation membrane resealing should have taken place within 1 min [6]. In our experiment, prior to the addition of PI, the sonicated cell samples from the cell chamber were first rinsed with RPMI medium twice to remove extracellular calcein, and then they were transferred to a 5-mL sterile round-bottom capped polystyrene tube (352054; BD Biosciences) whose shape is compatible with the flow cytometer's sample loading port. After that, PI was added to the cell-loaded polystyrene tube at 75-μm concentration and the cell samples were incubated for another 15 min. Subsequently, the cell samples were washed twice with PBS to remove extracellular PI and were fed with fresh RPMI medium. Note that PI is a red-fluorescent dye with excitation/emission maxima of 493/636 nm.

2) Flow Cytometry Protocol: To identify viable and sonoporated cells among a sonicated cell population, cell samples

were passed into an Aria III flow cytometer (BD Biosciences) by mounting the cell-loaded polystyrene tube onto the system's sample loading port and starting the cytometer's operation through its software console (FACSDiva; BD Biosciences). During the flow cytometry analysis, the fluorescence of calcein and PI was activated with a 488-nm laser, and the cells were gated based on their fluorescence level for the two dyes. From this bivariate analysis, sonicated cells in four categories were identified using built-in functions in the FACSDiva software environment: 1) viable and unsonoporated (calcein− and PI−); 2) viable and sonoporated (calcein+ and PI−); 3) nonviable and unsonoporated (calcein− and PI+); and 4) nonviable and sonoporated (calcein+ and PI+). Apart from the calcein/PI analysis, viable cells were also analyzed for their size and granularity with respect to sham-exposed cell samples. Such analysis was conducted as part of the flow cytometry analysis by examining the distributions of forward scatter (FSC) and side scatter (SSC) of a 488-nm laser beam as cells passed through the cytometer. FSC and SSC respectively provide information about the relative cell size and granularity of a population [52]. To avoid cell debris from confounding the acquired data, the flow cytometer was set to record a data point only if its FSC value was above 50 000 (an empirical threshold based on preliminary trials). Note that, in each flow cytometry run, data for 10^4 cells with FSC above the threshold was acquired at a rate of 300 events per second. Calcein fluorescence (green) was detected using a 530/30-nm bandpass filter, while PI fluorescence (red) was detected with a 616/23-nm filter. The gating boundaries for calcein and PI fluorescence (i.e., whether a cell was considered as calcein+ and PI+) were calibrated using baseline calcein and PI fluorescence values measured from sham-exposed cell samples which naturally yield negative calcein and PI fluorescence. For all experiments, data were downloaded for offline visualization in the form of population contour maps created using the WinList software (v. 7.0; Verity Software House, Topsham, ME, USA). To conduct statistical analysis, data for three independent flow cytometry runs were collected and each data set contained 10^4 cells, corresponding to $N = 4$ with 10^4 data points in each sample. The sample mean and standard deviation (SD) were calculated for different quantitative measures of the four sonicated cell categories using statistical analysis software (GraphPad Prism ver. 5; GraphPad Software, San Diego, CA, USA). Unpaired Student's t-test and one-way analysis of variance (ANOVA) were performed to assess statistical significance.

3) Confocal Microscopy Procedure: As comparisons to the flow cytometry assays, direct observations of post-exposure cellular fluorescence of calcein and PI were obtained using a live confocal microscope (LSM 710; Carl Zeiss, Jena, Germany). A 40× oil objective lens was used (numerical aperture: 1.3; refractive index: 1.518). Also, a 488-nm laser was used to excite the fluorescence of the two dyes, while filter bands of 500–540 and 610–650 nm were used, respectively for detecting the fluorescence emission of calcein and PI. As part of the procedure, bright-field images were captured in tandem to examine the morphology of sonicated cells.

IV. Demonstration Case Results

A. Variation in Cell Response to LIPUS Exposure

After receiving LIPUS exposure from our devised acoustic setup with MBs present in the cell chamber, a fraction of both leukemia cell types expectedly showed an increase in intracellular calcein fluorescence (an indication of sonoporation), while some exhibited a high expression of PI fluorescence (an indication of nonviability). Representative results are shown in Fig. 5 in the form of four-quadrant plots that show the calcein/PI bivariate distribution of a 10^4 sample population for each cell type (sham exposure and sonicated experiment trials were shown). As compared to sham exposure [Fig. 5(a) and (d)], whose cells show negative calcein and PI fluorescence in principle, the sonicated HL-60 population [Fig. 5(c)] and Molt-4 population [Fig. 5(f)] both had viable sonoporated cells (Q4; i.e., calcein+ and PI−), while some of the sonoporated cells became nonviable (Q2; i.e., calcein+ and PI+). Also, some sonicated cells remained viable yet unsonoporated (Q3; i.e., calcein− and PI−). In a few instances, the unsonoporated cells became nonviable after exposure (Q1; i.e., calcein− and PI+). In contrast, without the presence of MBs, the appearance of the four-quadrant plot was essentially similar to that for sham exposure [Fig. 5(b) and (e)], thereby, indicating that the LIPUS exposure on its own would not trigger sonoporation.

B. Variation in the Calcein Uptake Level of Viable Sonoporated Cells

Within the group of viable sonoporated cells, variations were found to exist in their calcein uptake level. As shown in Fig. 6(a) that shows histograms of calcein fluorescence for PI− cells, some sonoporated cells exhibited high calcein uptake, and we grouped these cells into a high uptake (HUP) cluster. In contrast, some sonoporated cells exhibited low calcein uptake, and they were grouped into a low uptake (LUP) cluster. These findings were found to correspond well with confocal microscopy observations that are shown in Fig. 6(b). This latter figure specifically showed that within a field of view encompassing a group of sonicated cells, LUP and HUP calcein+ cells can be found. Also, some calcein+ cells were concurrently PI+, signifying that they were nonviable.

C. More Sonicated HL-60 Cells Become Nonviable Than Molt-4 Cells When MBs were Present

Cell-type variation in cell viability (PI−) was found to exist between HL-60 and Molt-4 cells. As shown in Fig. 7, in the presence of MBs, sonicated HL-60 cells exhibited a significantly lower cell viability (13.4% less) than the sham-exposed cells ($p < 0.001$), while LIPUS exposure without MBs did not result in any substantial viability decline in HL-60 cells. On the other hand, sonicated Molt-4 cells, regardless of whether MBs were present, did not show a significant reduction in cell viability when comparing to the sham control group. Comparing between the two cell lines, it was found that the percentage of viable HL-60 cells after LIPUS exposure with MBs present was on average 13.1% lower than that for

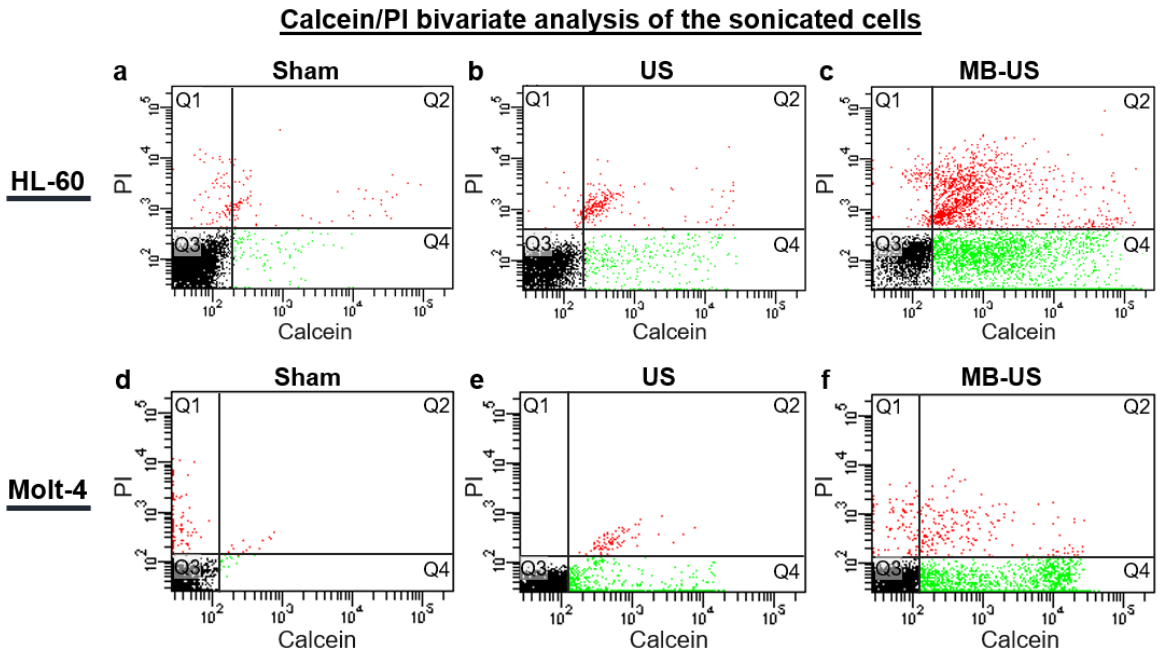

Fig. 5. Calcein/PI bivariate flow cytometry analysis of sonicated cells after exposure in four-quadrant plot. Cells in Q1 and Q2 represent the dead cells (PI+). Q3 represents the viable unsonoporated cells (PI−/calcein−). Q4 (PI−/calcein+) shows the viable sonoporated cells. (a) and (d) Data for sham-exposed cells respectively for HL-60 cells and Molt-4 cells. (b) and (e) Results of US exposure without the presence of MBs respectively for the two cell lines. (c) and (f) Data for the cells exposed by US in the presence of MB respectively for the two cell lines.

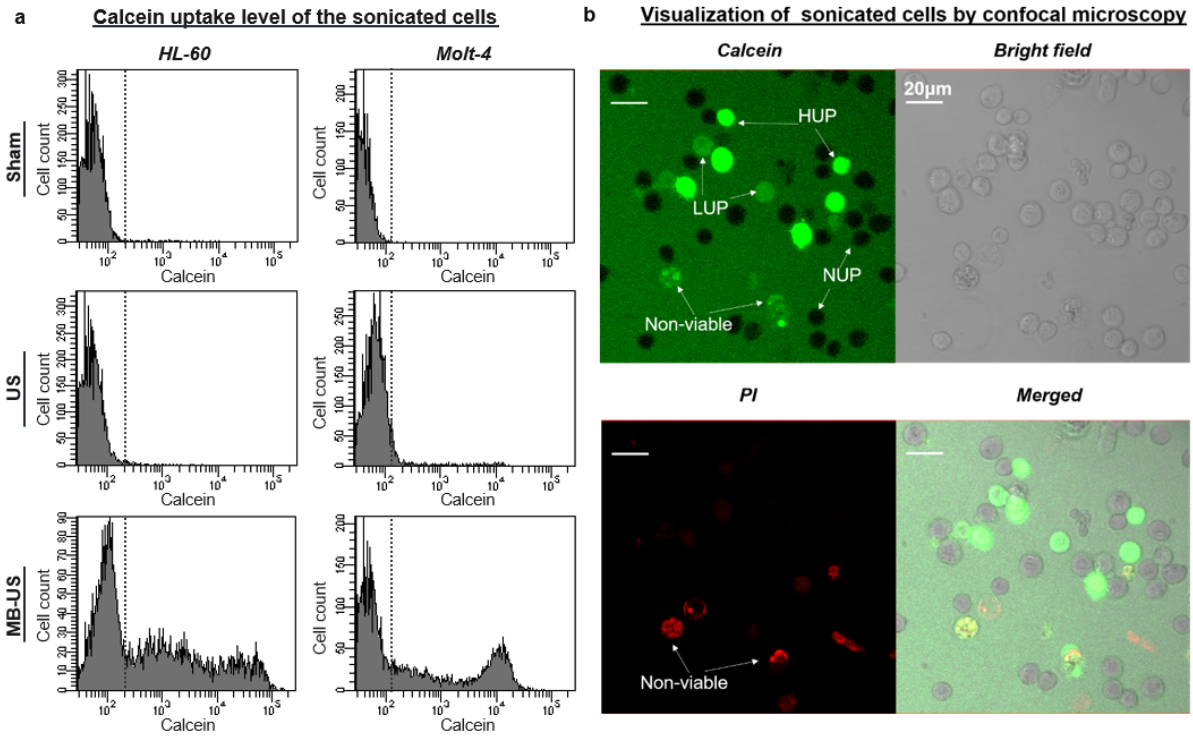

Fig. 6. Analysis of calcein uptake and cell viability after sonication. (a) Histograms showing the calcein distribution after exposure for HL-60 (column 1) and Molt-4 cells (column 2). The three rows show data for the sham-exposed, ultrasound without and with MBs, respectively. (b) Confocal imaging of an HL-60 cell sample after ultrasound exposure with MBs present. Upper left: channel of calcein. Lower left: channel of PI. Upper right: bright field image. Lower right: merge of the three channels. Examples of the post-exposure LUP, HUP, and nonviable cells were highlighted.

the viable Molt-4 cell population ($p < 0.001$). No statistically significant difference in cell viability was found between the sham-exposed groups of the two cell types, or between the two sonicated cell groups in the absence of MBs.

D. HL-60 Has Higher Sonoporation Rate Than Molt-4

With the same LIPUS exposure and the presence of MBs, the two leukemia cell lines showed a notable difference in the size of their sonoporated cell population (calcein+).

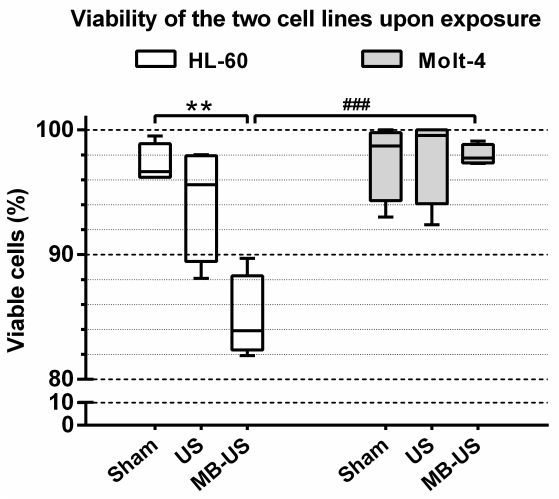

Fig. 7. Cell viability of the sonicated cells after exposure. Box plot shows the viable population of the sham-exposed, ultrasound without MBs, and ultrasound with MB groups for both HL-60 and Molt-4 cells. $** p < 0.01$ within same cell line; ### $p < 0.001$ between cell lines. $N = 4$.

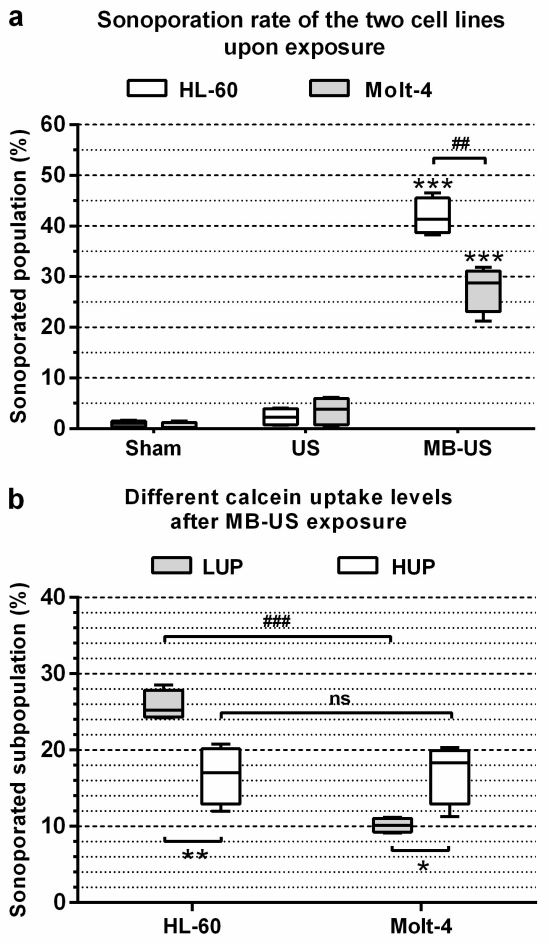

Fig. 8. Effects of sonication on sonoporation rate and calcein uptake level for HL-60 and Molt-4 cells. (a) Sonoporation rate of the two cell lines after exposure. (b) Distribution of LUP and HUP for both cell lines exposed by ultrasound in the presence of MBs. $* p < 0.05$, $** p < 0.01$, $*** p < 0.001$ within the same cell line; ## $p < 0.01$ and ### $p < 0.001$ between cell lines. $N = 4$.

As shown in Fig. 8(a), the percentage of sonoporated HL-60 cells was 13.4% higher than that of sonoporated Molt-4 cells ($p < 0.01$). On the other hand, without MBs, sonicated HL-60 and Molt-4 cells expectedly did not yield a statistically significant sonoporated cell population with respect to the sham control group.

For both cell lines, sonoporated cells that arose from LIPUS exposure in the presence of MBs exhibited LUP and HUP characteristics. As shown in Fig. 8(b), for HL-60, the LUP and HUP clusters respectively amounted to 25.9% and 16.8% of the sonicated cell population (LUP is 9.1% higher than HUP). On the other hand, for Molt-4, the size of the LUP cluster (10.1%) was found to be significantly lower than the size of the HUP cluster (17.1%). A statistically significant difference ($p < 0.001$) was also observed between the LUP cluster size for sonoporated HL-60 and Molt-4 cells.

E. HL-60 Cells with High Calcein Uptake Showed Decrease in Forward Scatter and Increase in Side Scatter

As additional data on the bioeffects induced by LIPUS and sonoporation, Fig. 9 (Columns 1 and 2) plots the FSC distributions (which give information on relative cell size) against calcein fluorescence for the two leukemia cell types. From these plots, it can be observed that for HL-60 cells, there is a left shift in the FSC distribution of the HUP cluster (Column 1, bottom row) as compared to that for the LUP cluster and unsonporated cells (which were calcein−). This trend indicates that sonoporated cells in the HUP cluster were smaller in size than those in the LUP cluster and unsonoporated cells. In contrast, such a trend was not apparent for Molt-4 cells. Also, no significant difference was found in the FSC distributions of the sham-exposed cells and sonicated cells without MBs.

The SSC distributions (which give the information on cellular granularity) for the two leukemia cell types are plotted in Columns 3 and 4 of Fig. 9. One key observation to be noted is that for the HUP cluster of sonoporated HL-60 cells, its SSC distribution (Column 3, bottom row) showed a right shift with respect to that for the LUP cluster and unsonoporated cells of the same type. This trend indicates an increase in the granularity of sonoporated HL-60 cells in the HUP cluster. On the other hand, no significant difference in the SSC distribution was found between sonoporated cells in the LUP cluster and unsonoporated population, nor was a significant difference observed between the SSC distributions of sham-exposed HL-60 cells and sonicated HL-60 cells without MBs. As for Molt-4 cells, no obvious difference was found in the SSC distributions of the sham-exposed group, sonicated group with MBs, and the two sonoporated cell clusters.

V. Discussion

A. Recap of Methodological Contributions

To properly study the bioeffects of LIPUS and sonoporation over a cell population, the meticulous design of the ultrasound exposure platform and the bioassay protocol are both essential to avoid confounding factors in the acquired observations. Previously, a wide range of ultrasound exposure platforms has been devised by different labs. However, many types of

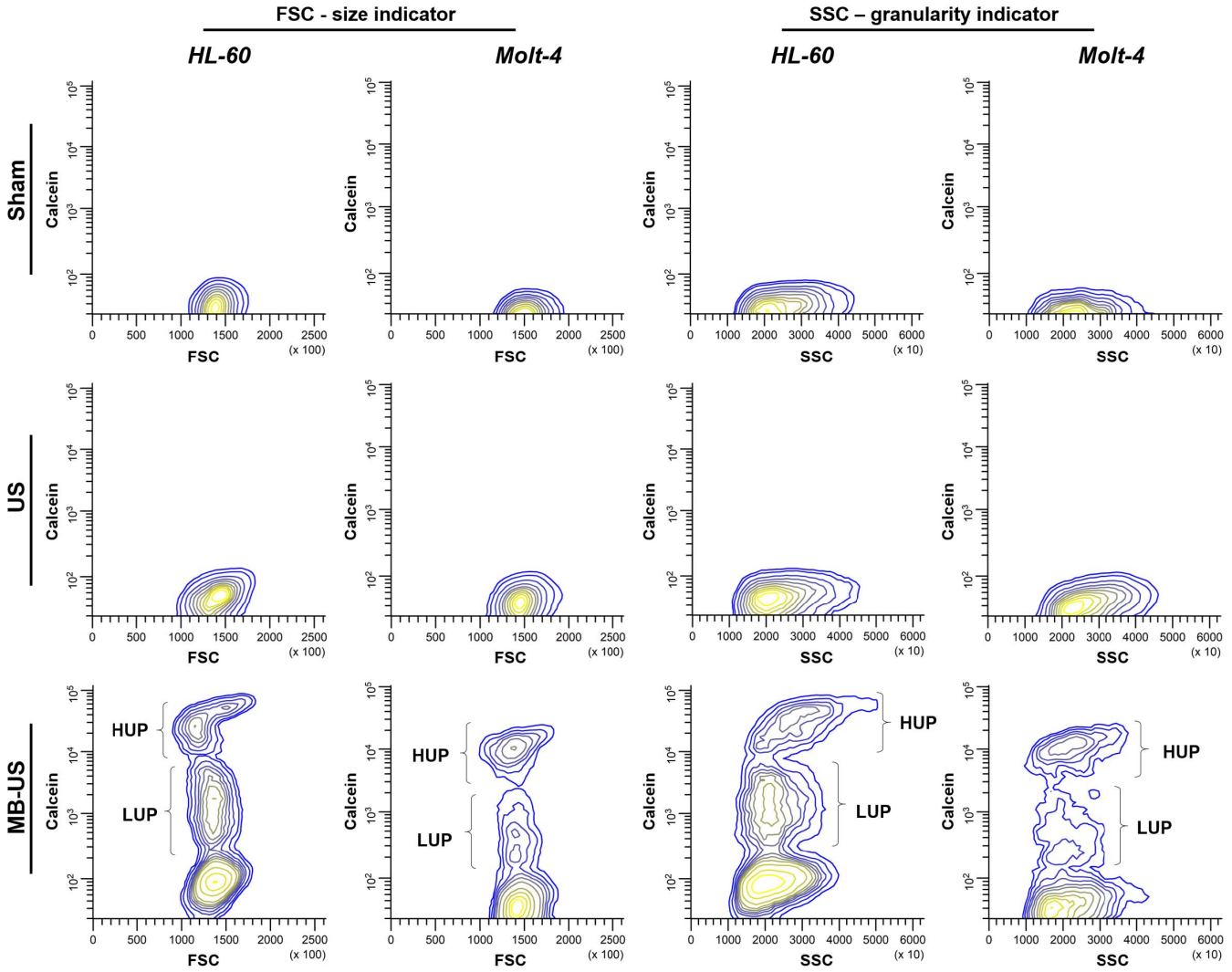

Fig. 9. Contour plots of the distributions of the viable populations after exposure for HL-60 and Molt-4 cells. The vertical axis represents the calcein level. The horizontal axis of columns 1 and 2 was the FSC indicating relative cell size, and of columns 3 and 4 was the SSC indicating relative granularity. Populations of LUP and HUP were marked in the groups exposed by ultrasound in the presence of MB for both cell lines.

exposure setups are known to have deficiencies. For setups that submerse the transducer directly into an open well containing a solution with cells and culture medium, they are subjected to a high risk of specimen contamination, and their acoustic field profile contains significant inhomogeneity [35]. Flaws are also present in exposure setups that separate the transducer from the cell chamber by a coupling gel layer or a water bath, because standing waves that exist in their generated acoustic field may represent a confounding factor in characterizing the ultrasound exposure being delivered to the specimen [36], [37]. To avoid the technical weaknesses of many existing ultrasound exposure platforms, an immersion-based setup (Figs. 1 and 2) can be designed as described in Section II. With such a setup, undesired wave reflections and acoustic field inhomogeneities are significantly reduced. Detailed field calibrations also ensured that the *in situ* ultrasound field was well characterized (Fig. 3) and the exposure levels were within the empirical limits (Table I) as recommended for ultrasound bioeffect studies.

Strong observations on the cellular bioeffects of LIPUS and sonoporation can be obtained if the key cell groups of interest (e.g., viable sonoporated cells) can be extracted from a sonicated cell population that might have received the same LIPUS exposure level but has exhibited variations in response between cells. As a demonstration case, a bioeffect experiment protocol has been presented in Section III (Fig. 4) to show how flow cytometry can be effectively leveraged to gate and identify sonicated cells based on their bivariate fluorescence expression related to sonoporation tracing (calcein) and viability (PI) (Fig. 5). Here, two leukemia cell lines (HL-60, Molt-4) were subjected to LIPUS exposure using our devised platform and a prescribed set of LIPUS parameters with 1-MHz ultrasound frequency, 1 kHz PRF, 10% duty cycle, 30-s exposure duration, 0.54-MPa peak negative pressure, 9.71 W/cm^2 I_{SPPA}, 0.97 W/cm^2 I_{SPTA}, and 29.1 J/cm^2 delivered acoustic energy density. MBs were added at 1:1 cell-to-bubble ratio and their presence was found to be critical to induce

sonoporation with the prescribed LIPUS parameters (Fig. 6). Some cell-type variations in bioeffects were observed to exist between HL-60 and Molt-4, including cell viability trends when MBs are present (Fig. 7), sonoporation rate (Fig. 8), and the morphology of viable sonoporated cells (Fig. 9). These variations are likely due to the difference in origin between HL-60 (a promyelocytic, malignant cell line) and Molt-4 (a T-lymphoblast differentiated malignant cell line).

B. Potential Protocol Modifications for Other Cellular Bioeffect Investigations

The cellular bioeffect investigation methodology reported in this paper can be readily extended to study other downstream bioeffects of sonicated cells. For instance, post-exposure apoptosis of sonicated cells may be identified with the use of fluorescent dyes such as Annexin-V that only binds to apoptotic cells. Also, cell-cycle progression delays of sonicated cells can be tracked with flow cytometry through a bromodeoxyuridine labeling approach [42]. As well, the behavior of subcellular events may be analyzed using fluorescent dyes such as JC-1 (to track mitrochondrial outer membrane potential) and ER-tracker (to study the mass of endoplasmic reticulum) [43]. These flow cytometry assays would yield more comprehensive findings on the downstream cellular impact of LIPUS and sonoporation.

Our experimental methodology may be applied to investigate other cell types too. One natural extension would be to deliver LIPUS to leukocytes that are readily found in the vasculature and study their bioeffects in the presence and absence of MBs. Such a study would yield insight on whether sonoporation would affect development kinetics of immune cells. Our protocol may also be easily updated to study the bioeffects of LIPUS on other established *in vitro* cell models, such as brain endothelial cells (for blood–brain barrier related studies) [53] and mesenchymal precursor cells (for mechanotransduction related studies) [54]. For these avenues of studies, our acoustic setup may be leveraged to conduct a parameter space analysis of different ultrasound exposure parameters. Moreover, new fluorescent markers may be added to the bioassay analysis to study potential bioeffects specific to those cell types, and other bioassay techniques such as Western blot analysis may be included to study cytoplasmic signaling protein expression. Note that, for studies that involve sonoporation, the timing for the addition of post-exposure viability tracer may be modified depending on the cell type being investigated. In the current form of our protocol, PI was added 5 min after sonication to label nonviable leukemia cells. This timing may need to be changed to 40 min after sonication (or even longer) when studying human erythrocytes, whose pore resealing time was found in electroporation experiments to be significantly longer than many other cell types [55]. Another point worth mentioning is that many cell types (e.g., endothelial cells) tend to grow in adherent cell layers. Nevertheless, it is not difficult to load such types of cells into the cell chamber of our setup, because trypsinization can be performed to resuspend adherent cell layers prior to loading, as explained elsewhere [42], [56].

It should be emphasized that the acoustic exposure parameters are not limited to the ones prescribed in our demonstration case. Transducers with other center frequencies may be readily used, and different pulsing parameters (PRF, pulse duration, exposure time) may be applied. Also, the spacing between platform panels on the acoustic exposure setup may be adjusted. If different acoustic parameters are to be used, it is important to recalibrate the ultrasound field conditions based on what is described in Section II-D and recalculate the exposure parameters as shown in Section II-E. Such measurements and calculations are essential to characterize the *in situ* exposure levels as required for ultrasound bioeffect experiments [19]. Regarding ultrasound field characterization, one caveat to be noted is that hydrophone-based field measurements inherently cannot gauge the ultrasound field at the cell chamber boundaries. If the boundary ultrasound field level needs to be examined, other characterization approaches such as computational simulations [35] and laser Doppler vibrometry [36] would need to be used. Nevertheless, hydrophone measurements can still practically depict the *in situ* ultrasound field of our exposure setup, since cell samples are often loaded into the cell chamber in suspension form as discussed in Section III.

VI. Conclusion

While the stimulatory effects of LIPUS and the acute impact of sonoporation on the cell membrane are now well-known, there has been a chronic shortage of knowledge on the related downstream bioeffects. In this paper, we have reported our group's approach to rationally devise an acoustic exposure platform with detailed exposure level characterization. Moreover, we have presented how a bioeffect experiment can be properly planned to make use of flow cytometry to obtain strong bioeffect observations that are specific to a certain cell group such as viable sonoporated cells. These methodological details can potentially serve as a helpful reference to other labs as they plan new cellular bioeffect experiments on LIPUS and sonoporation. In turn, they can help to boost the merit of bioeffect findings acquired in the future, thereby benefiting the overall quest to establish the therapeutic applicability of LIPUS and sonoporation.

References

[1] F. Ahmadi, I. V. McLoughlin, S. Chauhan, and G. ter Haar, "Bio-effects and safety of low-intensity, low-frequency ultrasonic exposure," *Prog. Biophys. Mol. Biol.*, vol. 108, no. 3, pp. 119–138, Apr. 2012.

[2] Z. Izadifar, P. Babyn, and D. Chapman, "Mechanical and biological effects of ultrasound: A review of present knowledge," *Ultrasound Med. Biol.*, vol. 43, no. 6, pp. 1085–1104, Jun. 2017.

[3] C. L. Romano, D. Romano, and N. Logoluso, "Low-intensity pulsed ultrasound for the treatment of bone delayed union or nonunion: A review," *Ultrasound Med. Biol.*, vol. 35, no. 4, pp. 529–536, Apr. 2009.

[4] F. Padilla, R. Puts, L. Vico, and K. Raum, "Stimulation of bone repair with ultrasound: A review of the possible mechanic effects," *Ultrasonics*, vol. 54, no. 5, pp. 1125–1145, Jul. 2014.

[5] V. F. Humphrey, "Ultrasound and matter—Physical interactions," *Prog. Biophys. Mol. Biol.*, vol. 93, pp. 195–211, Jan. 2007.

[6] Y. Hu, J. M. F. Wan, and A. C. H. Yu, "Membrane perforation and recovery dynamics in microbubble-mediated sonoporation," *Ultrasound Med. Biol.*, vol. 39, no. 12, pp. 2393–2405, Dec. 2013.

[7] S. R. Sirsi and M. A. Borden, "Advances in ultrasound mediated gene therapy using microbubble contrast agents," *Theranostics*, vol. 2, no. 12, pp. 1208–1222, Dec. 2012.

[8] H. D. Liang, J. Tang, and M. Halliwell, "Sonoporation, drug delivery, and gene therapy," *Proc. Inst. Mech. Eng. H, J. Eng. Med.*, vol. 224, no. 2, pp. 343–361, 2010.

[9] S. Ibsen, C. E. Schutt, and S. Esener, "Microbubble-mediated ultrasound therapy: A review of its potential in cancer treatment," *Drug Des. Develop. Ther.*, vol. 7, pp. 375–388, May 2013.

[10] M. Zacherl, G. Gruber, R. Radl, P. H. Rehak, and R. Windhager, "No midterm benefit from low intensity pulsed ultrasound after chevron osteotomy for hallux valgus," *Ultrasound Med. Biol.*, vol. 35, no. 8, pp. 1290–1297, Aug. 2009.

[11] P. M. de Albornoz, A. Khanna, U. G. Longo, F. Forriol, and N. Maffulli, "The evidence of low-intensity pulsed ultrasound for *in vitro,* animal and human fracture healing," *Brit. Med. Bull.*, vol. 100, no. 1, pp. 39–57, 2011.

[12] S. Schandelmaier *et al.*, "Low intensity pulsed ultrasound for bone healing: Systematic review of randomized controlled trials," *Brit. Med. J.*, vol. 356, Feb. 2017, Art. no. j656.

[13] E. Martin, "The cellular bioeffects of low intensity ultrasound," *Ultrasound*, vol. 17, no. 4, pp. 214–219, Nov. 2009.

[14] A. Moghaddam *et al.*, "Low intensity pulsed ultrasound in the treatment of long bone nonunions: Evaluation of cytokine expression as a tool for objectifying nonunion therapy," *J. Orthopaedics*, vol. 13, no. 4, pp. 306–312, Dec. 2016.

[15] A. Delalande, S. Kotopoulis, M. Postema, P. Midoux, and C. Pichon, "Sonoporation: Mechanistic insights and ongoing challenges for gene transfer," *Gene*, vol. 525, no. 2, pp. 191–199, 2013.

[16] Y. Liu, J. Yan, and M. R. Prausnitz, "Can ultrasound enable efficient intracellular uptake of molecules? A retrospective literature review and analysis," *Ultrasound Med. Biol.*, vol. 38, no. 5, pp. 876–888, May 2012.

[17] I. Lentacker, I. De Cock, R. Deckers, S. C. De Smedt, and C. T. W. Moonen, "Understanding ultrasound induced sonoporation: Definitions and underlying mechanisms," *Adv. Drug Del. Rev.*, vol. 72, pp. 49–64, Jun. 2014.

[18] P. Qin, T. Han, A. C. H. Yu, and L. Xu, "Mechanistic understanding the bioeffects of ultrasound-driven microbubbles to enhance macromolecule delivery," *J. Control. Release*, vol. 272, pp. 169–181, Feb. 2018.

[19] G. ter Haar *et al.*, "Guidance on reporting ultrasound exposure conditions for bio-effects studies," *Ultrasound Med. Biol.*, vol. 37, no. 2, pp. 177–183, Feb. 2011.

[20] Y. Hu, W. Zhong, J. M. Wan, and A. C. Yu, "Ultrasound can modulate neuronal development: Impact on neurite growth and cell body morphology," *Ultrasound Med. Biol.*, vol. 39, no. 5, pp. 915–925, May 2013.

[21] Y. Hu, J. M. F. Wan, and A. C. H. Yu, "Cytomechanical perturbations during low-intensity ultrasound pulsing," *Ultrasound Med. Biol.*, vol. 40, no. 7, pp. 1587–1598, Jul. 2014.

[22] C. D. Ohl *et al.*, "Sonoporation from jetting cavitation bubbles," *Biophys. J.*, vol. 91, pp. 4285–4295, Dec. 2006.

[23] F. Yuan, C. Yang, and P. Zhong, "Cell membrane deformation and bioeffects produced by tandem bubble-induced jetting flow," *Proc. Nat. Acad. Sci. USA*, vol. 112, pp. 7039–7047, Dec. 2015.

[24] N. Kudo, "High-speed *in situ* observation system for sonoporation of cells with size- and position-controlled microbubbles," *IEEE Trans. Ultrason., Ferroelectr., Freq. Control*, vol. 64, no. 1, pp. 273–280, Jan. 2017.

[25] X. Chen, R. S. Leow, Y. Hu, J. M. F. Wan, and A. C. H. Yu, "Single-site sonoporation disrupts actin cytoskeleton organization," *J. Roy. Soc. Interface*, vol. 11, no. 95, 2014, Art. no. 20140071.

[26] R. S. Leow, J. M. F. Wan, and A. C. H. Yu, "Membrane blebbing as a recovery manoeuvre in site-specific sonoporation mediated by targeted microbubbles," *J. Roy. Soc. Interface*, vol. 12, no. 105, 2015, Art. no. 20150029.

[27] B. Helfield, X. Chen, S. C. Watkins, and F. S. Villanueva, "Biophysical insight into mechanisms of sonoporation," *Proc. Nat. Acad. Sci. USA*, vol. 113, no. 36, pp. 9983–9988, 2016.

[28] N. Kudo, K. Okada, and K. Yamamoto, "Sonoporation by single-shot pulsed ultrasound with microbubbles adjacent to cells," *Biophys. J.*, vol. 96, no. 12, pp. 4866–4876, 2009.

[29] Z. Fan, H. Liu, M. Mayer, and C. X. Deng, "Spatiotemporally controlled single cell sonoporation," *Proc. Nat. Acad. Sci. USA*, vol. 109, pp. 16486–16491, Oct. 2012.

[30] F. Li *et al.*, "Dynamics and mechanisms of intracellular calcium waves elicited by tandem bubble-induced jetting flow," *Proc. Nat. Acad. Sci. USA*, vol. 115, pp. E353–E362, Jan. 2018.

[31] P. Qin *et al.*, "Sonoporation-induced depolarization of plasma membrane potential: Analysis of heterogeneous impact," *Ultrasound Med. Biol.*, vol. 40, no. 5, pp. 979–989, May 2014.

[32] C. Jia, L. Xu, T. Han, P. Cai, A. C. H. Yu, and P. Qin, "Generation of reactive oxygen species in heterogeneously sonoporated cells by microbubbles with single-pulse ultrasound," *Ultrasound Med. Biol.*, vol. 44, no. 5, pp. 1074–1085, May 2018.

[33] Y. Zhou, R. E. Kumon, J. Cui, and C. X. Deng, "The size of sonoporation pores on the cell membrane," *Ultrasound Med. Biol.*, vol. 35, no. 10, pp. 1756–1760, Oct. 2009.

[34] A. Alassaf, A. Aleid, and V. Frenkel, "*In vitro* methods for evaluating therapeutic ultrasound exposures: Present-day models and future innovations," *J. Therapeutic Ultrasound*, vol. 1, Nov. 2013, Art. no. 21.

[35] K. Hansel, M. P. Mienkina, and G. Schmitz, "Analysis of ultrasound fields in cell culture wells for *in vitro* ultrasound therapy experiments," *Ultrasound Med. Biol.*, vol. 37, no. 12, pp. 2105–2115, Dec. 2011.

[36] J. J. Leskinen and K. Hynynen, "Study of factors affecting the magnitude and nature of ultrasound exposure with *in vitro* set-ups," *Ultrasound Med. Biol.*, vol. 38, no. 5, pp. 777–794, May 2012.

[37] W. Secomski, K. Bilmin, T. Kujawska, A. Nowicki, P. Grieb, and P. A. Lewin, "*In vitro* ultrasound experiments: Standing wave and multiple reflections influence on the outcome," *Ultrasonics*, vol. 77, pp. 203–213, May 2017.

[38] J. A. Kopechuk, H. Kim, D. D. McPherson, and C. K. Holland, "Calibration of the 1-MHz Sonitron ultrasound system," *Ultrasound Med. Biol.*, vol. 36, no. 10, pp. 1285–1295, Oct. 2010.

[39] H. R. Guzman, D. X. Nguyen, S. Khan, and M. R. Prausnitz, "Ultrasound-mediated disruption of cell membranes. II. Heterogeneous effects on cells," *J. Acoust. Soc. Amer.*, vol. 110, pp. 597–606, Jul. 2001.

[40] A. C. H. Yu and J. A. Hossack, "Methods and protocols: Engine for the next wave of biomedical ultrasound innovations," *IEEE Trans. Ultrason., Ferroelectr., Freq. Control*, vol. 64, no. 1, pp. 6–10, Jan. 2017.

[41] H. R. Guzman, A. J. McNamara, D. X. Nguyen, and M. R. Prausnitz, "Bioeffects caused by changes in acoustic cavitation bubble density and cell concentration: A unified explanation based on cell-to-bubble ratio and blast radius," *Ultrasound Med. Biol.*, vol. 29, no. 8, pp. 1211–1222, Aug. 2003.

[42] X. Chen, J. M. F. Wan, and A. C. H. Yu, "Sonoporation as a cellular stress: Induction of morphological repression and developmental delays," *Ultrasound Med. Biol.*, vol. 39, no. 6, pp. 1075–1086, Jun. 2013.

[43] W. Zhong, X. Chen, P. Jiang, J. M. F. Wan, P. Qin, and A. C. H. Yu, "Induction of endoplasmic reticulum stress by sonoporation: Linkage to mitochondria-mediated apoptosis initiation," *Ultrasound Med. Biol.*, vol. 39, no. 12, pp. 2382–2392, Dec. 2013.

[44] F. A. Duck, "Medical and non-medical protection standards for ultrasound and infrasound," *Progr. Biophys. Mol. Biol.*, vol. 93, nos. 1–3, pp. 176–191, 2007.

[45] T. G. Leighton, "What is ultrasound?" *Prog. Biophys. Mol. Biol.*, vol. 93, nos. 1–3, pp. 3–83, Jan./Apr. 2007.

[46] D. Wolf and V. Rotter, "Major deletions in the gene encoding the p53 tumor antigen cause lack of p53 expression in HL-60 cells," *Proc. Nat. Acad. Sci. USA*, vol. 82, pp. 790–794, Feb. 1985.

[47] G. del Bino, J. S. Skierski, and Z. Darzynkiewicz, "Diverse effects of camptothecin, an inhibitor of topoisomerase I, on the cell cycle of lymphocytic (L1210, MOLT-4) and myelogenous (HL-60, KG1) leukemic cells," *Cancer Res.*, vol. 50, pp. 5746–5750, 1990.

[48] F. Traganos, B. Ardelt, N. Halko, S. Bruno, and Z. Darzynkiewicz, "Effects of genistein on the growth and cell cycle progression of normal human lymphocytes and human leukemic MOLT-4 and HL-60 cells," *Cancer Res.*, vol. 52, pp. 6200–6208, Nov. 1992.

[49] H. R. Guzman, D. X. Nguyen, A. J. Mcnamara, and M. R. Prausnitz, "Equilibrium loading of cells with macromolecules by ultrasound: Effects of molecular size and acoustic energy," *J. Pharmaceutical Sci.*, vol. 91, no. 7, pp. 1693–1701, Jul. 2002.

[50] S. M. Fix, A. Novell, Y. Yun, P. A. Dayton, and C. B. Arena, "An evaluation of the sonoporation potential of low-boiling point phase-change ultrasound contrast agents *in vitro*," *J. Therapeutic Ultrasound*, vol. 5, no. 7, pp. 1–11, 2017.

[51] P. Qin, L. Xu, T. Han, L. Du, and A. C. H. Yu, "Effect of non-acoustic parameters on heterogeneous sonoporation mediated by single-pulse ultrasound and microbubbles," *Ultrason. Sonochem.*, vol. 31, pp. 107–115, Jul. 2016.

[52] A. Adan, G. Alizada, Y. Kiraz, Y. Baran, and A. Nalbant, "Flow cytometry: Basic principles and applications," *Crit. Rev. Biotechnol.*, vol. 37, no. 2, pp. 163–176, 2017.

[53] S. Lelu *et al.*, "Primary porcine brain endothelial cells as *in vitro* model to study effects of ultrasound and microbubbles on blood-brain barrier function," *IEEE Trans. Ultrason., Ferroelectr., Freq. Control*, vol. 64, no. 1, pp. 281–290, Jan. 2017.
[54] R. Puts *et al.*, "Activation of mechanosensitive transcription factors in murine C2C12 mesenchymal precursors by focused low-intensity pulsed ultrasound (FLIPUS)," *IEEE Trans. Ultrason., Ferroelectr., Freq. Control*, vol. 63, no. 10, pp. 1505–1513, Oct. 2016.
[55] G. Saulis, M. S. Venslauskas, and J. Naktinis, "Kinetics of pore resealing in cell membranes after electroporation," *J. Electroanal. Chem. Interfacial Chem.*, vol. 321, no. 1, pp. 1–13, Aug. 1991.
[56] H. R. Guzman, D. X. Nguyen, S. Khan, and M. R. Prausnitz, "Ultrasound-mediated disruption of cell membranes. I. Quantification of molecular uptake and cell viability," *J. Acoust. Soc. Amer.*, vol. 110, pp. 588–596, Jul. 2001.

Xinxing Duan received the B.Sc. degree in physics from the Huazhong University of Science and Technology, Wuhan, China, in 2008, the M.Phil. degree in mechanical and automation engineering from the Chinese University of Hong Kong, Hong Kong, in 2014, and the Ph.D. degree in biology from The University of Hong Kong, Hong Kong, in 2018.

She is currently a Post-Doctoral Fellow with the Department of Electrical and Computer Engineering at University of Waterloo, Waterloo, ON, Canada, and an Associate Scientist with the Laboratory on Innovative Technology in Medical Ultrasound at Schlegel Research Institute for Aging, Waterloo. Her research interest is in therapeutic ultrasound, specifically in devising innovative drug delivery applications as well as in investigating wave-cell interactions and related biophysical processes.

Alfred C. H. Yu (S'99–M'07–SM'12) received the B.Sc. degree in electrical engineering from the University of Calgary, Calgary, AB, Canada, in 2002, and the M.A.Sc. and Ph.D. degrees from the University of Toronto, Toronto, ON, Canada, in 2004 and 2007, respectively.

From 2007 to 2015, he was the Founder and the Principal Investigator of the Biomedical Ultrasound Laboratory at The University of Hong Kong, Hong Kong. In 2015, he joined the University of Waterloo, Waterloo, ON, as an Associate Professor. Since 2018, he has been a Full Professor at the University of Waterloo. He has long-standing research interests in ultrasound imaging and therapeutics.

Dr. Yu is an Editorial Board Member of Ultrasound in Medicine and Biology, the Chair of the Medical Ultrasound Technical Program Committee of the IEEE Ultrasonics Symposium, and a Board Member of the International Society for Therapeutic Ultrasound. He was a recipient of the IEEE Ultrasonics Early Career Investigator Award, the Frederic Lizzi Early Career Award, and the Ontario Early Researcher Award. He is an Associate Editor-in-Chief of the IEEE TRANSACTIONS ON ULTRASONICS, FERROELECTRICS, AND FREQUENCY CONTROL.

Jennifer M. F. Wan received the B.Sc. degree in biology and chemistry from the University of London, London, U.K., in 1983, and the Ph.D. degree from the University of Southampton, Southampton, U.K., in 1987.

She started her academic career at Harvard Medical School, Boston, MA, USA, as an Instructor of Medicine. Since 1993, she has been with the School of Biological Sciences, The University of Hong Kong, Hong Kong, as a Tenured Associate Professor. Her research interests include ultrasound-induced cellular phenomena, proteomics, Chinese medicine, and nutritional science.

Dr. Wan was the Founding President of the Hong Kong Society of Flow Cytometry and the Chairperson of the Hong Kong Food Science and Technology Association.